University Library



A gateway to Melbourne's research publications

Minerva Access is the Institutional Repository of The University of Melbourne

Author/s:
Bode, S;Bennett, D;Sewell, DK;Paton, B;Egan, GF;Smith, PL;Murawski, C

Title:
Dissociating neural variability related to stimulus quality and response times in perceptual decision-making

Date:
2018-03-01

Citation:
Bode, S., Bennett, D., Sewell, D. K., Paton, B., Egan, G. F., Smith, P. L. & Murawski, C. (2018). Dissociating neural variability related to stimulus quality and response times in perceptual decision-making. Neuropsychologia, 111, pp.190-200. https://doi.org/10.1016/j.neuropsychologia.2018.01.040.

Persistent Link:
https://hdl.handle.net/11343/300039

Neuropsychologia 111 (2018) 190–200

Contents lists available at ScienceDirect

Neuropsychologia

journal homepage: www.elsevier.com/locate/neuropsychologia

Dissociating neural variability related to stimulus quality and response times in perceptual decision-making

Stefan Bode[a,b,*], Daniel Bennett[a,c,d], David K. Sewell[a,e], Bryan Paton[f,g,h,i], Gary F. Egan[f,g,h], Philip L. Smith[a], Carsten Murawski[c]

[a] Melbourne School of Psychological Sciences, The University of Melbourne, Australia
[b] Department of Psychology, University of Cologne, Germany
[c] Department of Finance, The University of Melbourne, Australia
[d] Princeton Neuroscience Institute, Princeton University, NJ, USA
[e] School of Psychology, The University of Queensland, Australia
[f] Monash Biomedical Imaging, Monash University, Australia
[g] School of Psychological Sciences, Monash University, Australia
[h] ARC Centre of Excellence for Integrative Brain Function, Monash University, Australia
[i] School of Psychology, The University of Newcastle, Australia

ARTICLE INFO

Keywords:
Perceptual decision-making
Evidence accumulation
Functional magnetic resonance imaging
Sequential sampling models
Decision difficulty

ABSTRACT

According to sequential sampling models, perceptual decision-making is based on accumulation of noisy evidence towards a decision threshold. The speed with which a decision is reached is determined by both the quality of incoming sensory information and random trial-by-trial variability in the encoded stimulus representations. To investigate those decision dynamics at the neural level, participants made perceptual decisions while functional magnetic resonance imaging (fMRI) was conducted. On each trial, participants judged whether an image presented under conditions of high, medium, or low visual noise showed a piano or a chair. Higher stimulus quality (lower visual noise) was associated with increased activation in bilateral medial occipito-temporal cortex and ventral striatum. Lower stimulus quality was related to stronger activation in posterior parietal cortex (PPC) and dorsolateral prefrontal cortex (DLPFC). When stimulus quality was fixed, faster response times were associated with a positive parametric modulation of activation in medial prefrontal and orbitofrontal cortex, while slower response times were again related to more activation in PPC, DLPFC and insula. Our results suggest that distinct neural networks were sensitive to the quality of stimulus information, and to trial-to-trial variability in the encoded stimulus representations, but that reaching a decision was a consequence of their joint activity.

1. Introduction

Everyday perceptual decisions are generally made quickly and without conscious deliberation. These decisions involve comparing the sensory representations of objects encountered in the environment to memory representations of potential decision options. Making accurate perceptual decisions allows us to choose appropriate actions and behavioural responses. There has been intensive research into cognitive models underlying perceptual decisions (e.g., Bogacz et al., 2006; Brown and Heathcote, 2008; Forstmann et al., 2016; Purcell et al., 2010; Luce, 1986; Ratcliff, 1978; Smith and Ratcliff, 2004; Townsend and Ashby, 1983; Usher and McClelland, 2001; Vickers, 1979). A variety of models have been proposed that share the general idea that noisy evidence is accumulated over time until a decision threshold (criterion/boundary) is reached. Such models are known as *sequential-sampling models* (Ratcliff and Smith, 2004; Sewell and Smith, 2016; Smith and Ratcliff, 2015). These models assume that response time (RT) and accuracy depend jointly on (1) the quality of cognitive representation of the stimulus, which determines the rate at which evidence accumulates, and (2) the setting of decision threshold(s), which control how much evidence is needed before making a response. In this article, we use the diffusion decision model framework (DDM; Ratcliff, 1978; Ratcliff and McKoon, 2008) to investigate the neural correlates of perceptual decision making. The DDM has provided an account of decision-making in a variety of cognitive tasks and of the individual difference parameters that distinguish between participant populations in

* Correspondence to: Decision Neuroscience Laboratory, Melbourne School of Psychological Sciences, The University of Melbourne, Parkville, VIC 3010, Australia.
E-mail address: sbode@unimelb.edu.au (S. Bode).

https://doi.org/10.1016/j.neuropsychologia.2018.01.040
Received 2 October 2017; Received in revised form 25 January 2018; Accepted 27 January 2018
Available online 01 February 2018
0028-3932/ © 2018 Elsevier Ltd. All rights reserved.

a variety of task environments (Ratcliff et al., 2015, 2016).

The DDM and other sequential-sampling models assume that trial-to-trial variability in RT and decision outcome depends on both systematic and random factors. Decision outcomes and their associated RTs depend systematically on the *quality of stimulus information,* which determines the rate at which evidence accumulates. In the DDM, the rate of evidence accumulation is termed the *drift rate*. If the quality of the stimulus information is high, then evidence will quickly and consistently accumulate towards the appropriate decision threshold. RTs are also assumed to depend systematically on the settings of decision thresholds for evidence accumulation, which are typically the same (on average) for all stimuli within an experimental block. In addition to these systematic factors, the evidence accumulation process can be perturbed by random factors, conceptualised as *noise* within the system. Noise can be external to the decision-maker (e.g., variability in the exact number of photons reaching the retina) or internal (e.g., random fluctuations in neural processing). The DDM assumes two sources of noise that affect evidence accumulation: One is trial-to-trial (or across-trial) variability; the other is moment-to-moment (or within-trial) variability. Across-trial variability reflects variability in the encoded representations of nominally equivalent stimuli. Within-trial variability represents momentary fluctuations in the neural mechanism that represents the accumulating evidence. The combined effect of these sources of noise on the evidence accumulation process is to introduce variability into the decision outcome and the RT. One presentation of a particular stimulus may lead to a fast and accurate response; another presentation of the same stimulus on a later trial may lead to a slow and/or inaccurate response.

Despite substantial progress in refining cognitive models of the decision-making process, the neural mechanisms underlying these evidence accumulation dynamics are still debated. Electrophysiology studies (for reviews see Gold and Shadlen, 2007; Romo and de Lafuente, 2013; Shadlen and Kiani, 2013) have provided evidence for a role of early sensory regions in decision-making for simple stimuli presented in different sensory modalities, including visual motion (Britten et al., 1996; Ditterich et al., 2003), tactile vibration (Romo and Salinas, 2003), and auditory stimuli of different frequencies (Tsunada et al., 2016). However, neurons in brain regions not specifically related to sensory processing have also exhibited response profiles that more directly reflect decision-making activity; e.g., the lateral intraparietal (LIP) area (Bennur and Gold, 2011; Huk et al., 2017; Roitman and Shadlen, 2002; Shadlen and Newsome, 2001), the basal ganglia (Ding and Gold, 2012, 2013) and regions involved in response preparation such as the pre-motor cortex (for button-press responses) and frontal eye fields (for saccade responses) (Gold and Shadlen, 2000; Kim and Shadlen, 1999; Selen et al., 2012; Hanks et al., 2015).

Experiments in humans using functional magnetic resonance imaging (fMRI) have also revealed an extensive network of regions involved in various stages of the decision process (for reviews see Heekeren et al., 2008; Philiastides and Heekeren, 2009; for a meta-analysis see Keuken et al., 2014). These studies also found decision-related activation in early sensory brain regions (e.g., Binder et al., 2004; Pleger et al., 2006, Serences and Boynton, 2007). Decisions about more complex visual objects have been shown to involve specialised visual regions, such as face-processing regions in inferotemporal cortex for face decisions and the lateral occipital complex (LOC) for other object decisions (e.g., Bode et al., 2012a, 2013; Heekeren et al., 2004; Tremel and Wheeler, 2015; Williams et al., 2007). It remains to be understood, however, how sensory evidence for competing choice alternatives, possibly encoded in different brain regions, is combined into one dynamically evolving unified signal that could be interpreted as a decision variable. Different regions have been suggested to fulfil such a role, including the dorsolateral prefrontal cortex (DLPFC) (Heekeren et al., 2004, 2006), the insula (Ho et al., 2009; Liu and Pleskac, 2011), and a wider network of inferior temporal, frontal and parietal regions (Hebart et al., 2012, 2016; Kayser et al., 2010a, 2010b; Ploran et al., 2007; Tosoni et al., 2008). Others have suggested that activity in some regions, including the anterior insula, anterior cingulate cortex (ACC) and DLPFC, reflects task difficulty rather than the decision process itself (Philiastides and Sajda, 2006, 2007; Philiastides et al., 2006). Several sub-cortical regions, including the basal ganglia and the subthalamic nucleus, have also been identified as part of a cortically modulated network, subserving functions such as cautiousness-moderated threshold setting, and switching from evidence accumulation to action preparation (Bogacz and Gurney, 2007; Herz et al., 2016; Forstmann et al., 2008).

Our study sought to investigate the roles of these different brain regions by disentangling two factors that were not adequately accounted for in many previous studies (with some notable exceptions; e.g., Tremel and Wheeler, 2015): *stimulus quality* and *trial-to-trial variability in the encoded representations of stimuli*, as indexed by variability in response times for fixed levels of stimulus quality. We use the term “stimulus quality” to refer to the nominal, or objective, discriminability of the stimulus, as defined by the experimenter. Trial-to-trial variability in the encoded representations encompasses the cumulative effects of noise during individual experimental trials that affect the discriminability of the presented stimulus on that particular trial. The effect of such variability can render the difficulty of the decision on any trial either easier or harder than its nominal value. We implemented a simple choice task in which participants were required to make a series of perceptual decisions between images from two object categories, pianos and chairs, that have been used successfully in previous studies (Bode et al., 2012a, 2012b, 2013), presented under different levels of discriminability (i.e., stimulus quality). Specifically, we aimed to clarify the role of object-processing visual regions as well as prefrontal and parietal brain regions, the insula and the basal ganglia. Some of these regions might be better understood as reflecting the quality of the information used to drive evidence accumulation during decision-making, while others might reflect the influence of trial-to-trial variability on the encoded representations (i.e., the effects of external and internal noise on decision information). We used a parametric regression approach for fMRI data to simultaneously search for brain regions in which activation levels were positively or negatively correlated with stimulus quality. In a second step, we searched for brain regions in which, under fixed levels of stimulus quality, activation was positively correlated with RT (slower decisions) and negatively correlated with RT (faster decisions), reflecting the influence of noise on discriminability. This approach further allowed us to investigate two aspects of “task difficulty”, namely, difficulty due to experimenter-controlled stimulus discriminability, and difficulty due to the presence of random noise on a given trial. In a last step, we correlated neural activation, which showed the respective parametric modulation with either stimulus quality or RT for fixed stimulus quality levels with various parameters of the DDM.

2. Materials and methods

2.1. Participants

Twenty-six participants took part in the study. Three data sets were not recorded due to technical problems with the acquisition hardware. The final sample consisted of 23 participants (10 female, 13 male; mean age 23.7 years, range 19–36 years). Participants were recruited via advertisements at the University of Melbourne and Monash University. They had no history of neurological disorders, no contra-indicators for fMRI, were right-handed, and had normal or corrected-to-normal visual acuity. All participants gave written informed consent before participation, and they were compensated for their time with AUD 40. The study was approved by the human research ethics committee of Monash University (CF12/1399–2012000734), Australia, and conducted in accordance with the Declaration of Helsinki.

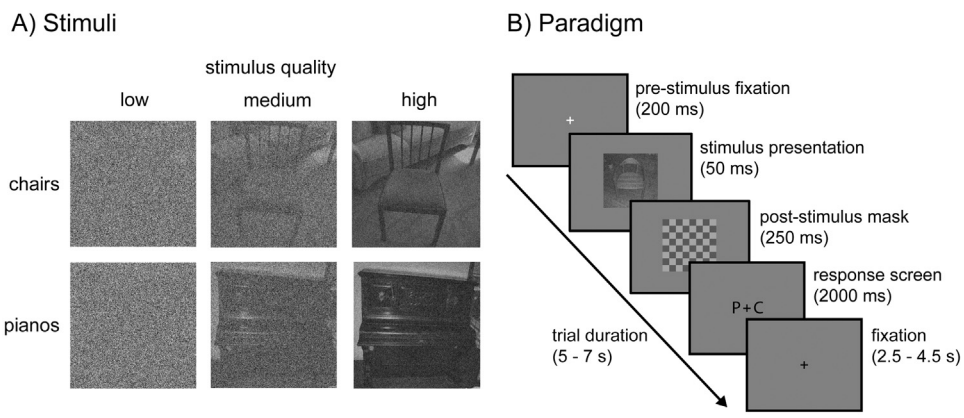

Fig. 1. Stimuli and paradigm. A) Stimuli. Twelve images of chairs and twelve images of pianos were used and presented at three levels of discriminability. Salt-and-pepper visual noise was added to achieve differences in stimulus quality. Visual noise levels were calculated individually before each block, depending on performance in the previous block, in order to achieve approximately 50% (low stimulus quality), 70% (medium stimulus quality) and 90% (high stimulus quality) correct decisions. B) Paradigm. In each trial, one of the stimuli was presented, followed by a short checkerboard mask to terminate visual processing. The mapping of stimulus categories to motor responses was randomised each trial. Each image was presented once per run at each discriminability level (72 trials in total per run), together with 8 interspersed null trials (5–7 s fixation), in an individually pseudo-randomised order. The experiments comprised six runs.

2.2. Stimuli and experimental procedure

Stimuli were twelve grey-scale images (400 × 400 pixels) of pianos and twelve images of chairs (Bode et al., 2012a, 2012b, 2013), created from freely available pictures from the Internet and custom-made photographs, showing the objects in front of different natural backgrounds (Fig. 1A). Images were presented on a light-grey background. Salt-and-pepper visual noise (a random selection of black and white pixels) was superimposed at different density levels to create three levels of discriminability (i.e., stimulus quality). Visual noise for the high stimulus quality condition was minimal and held constant for all participants and yielded ~ 90% correct decisions in pre-tests. Visual noise level for the low stimulus quality condition was very high and also held constant to yield chance level performance of ~ 50%. Visual noise levels in the medium stimulus quality condition were adjusted on a run-by-run and participant-by-participant basis in response to each individual's decision performance in the previous experimental run to yield ~ 70% correct decisions. Adjustments were made using the QUEST staircase algorithm (Watson and Pelli, 1983). For the first experimental run, performance in a calibration run prior to the experiment was used to calculate visual noise levels for this condition. Stimulus presentation was always followed by the same checkerboard mask, of equal size to the stimulus and consisting of 8 × 8 medium-contrast light and dark squares, to prevent further visual processing.

After a short fixation period (white fixation cross for 200 ms), one of the 24 stimuli was presented at one of the three possible stimulus quality levels for 50 ms. This was followed by the checkerboard mask (250 ms), and subsequently by the response screen (2000 ms), which displayed the letters “P” (piano) and “C” (chair) on either the left or right hand side of the fixation cross (Fig. 1B). The mapping of categories and response buttons was randomised for each trial in order to decorrelate choices from motor responses (Bode et al., 2012a, 2012b, 2013). Participants indicated their response by pressing either the left or the right response button of an MRI-compatible Cedrus button box using the index- and middle finger of the right hand. Participants made a response on each trial, and were encouraged to make their best guess if they were unsure. After a jittered fixation period, drawn from a uniform distribution of 2.5 s, 3.5 s, and 4.5 s, the next trial started.

The experiment was divided into six separate runs. Each of the 24 stimuli (12 piano images and 12 chair images) was presented at each of the three discriminability levels once in each run, yielding 72 trials per run in total (i.e., 24 trials per discriminability level). Eight additional null trials of the same length were randomly interspersed in each run in which only the fixation cross was shown, allowing for a better estimation of the hemodynamic response function (HRF). Each run lasted eight minutes, and participants could take short breaks between runs. All stimuli were presented in MATLAB (The Mathworks; Natick, MA) using the Psychophysics Toolbox (Brainard, 1997).

2.3. fMRI data acquisition

A Siemens 3T Skyra scanner (Erlangen, Germany) was used to acquire 172 functional images (echo planar imaging, EPI) in six experimental runs. A standard 32-channel head coil was used, and 42 axial slices covering the whole brain were acquired. The repetition time (TR) was 2800 ms, the echo time (TE) was 30 ms, the flip angle was 90 degrees, and the voxel resolution was 3 × 3 × 3 mm without gap. The first three images of each run were discarded by default to allow for magnetic saturation effects. In addition, T1 weighted-images (voxel size 0.9 × 0.9 × 0.9 mm; TR 1900 ms; TE 2.49 ms) were acquired for co-registration for each participant.

2.4. fMRI data analysis

All data were pre-processed using standard procedures as implemented in SPM8 (http://www.fil.ion.ucl.ac.uk/spm/). EPIs were realigned to the first image of the first run in order to correct for head motion. The EPIs were then slice-timing corrected, normalised to the Montreal Neurological Institute (MNI) template, and spatially smoothed with a Gaussian kernel of 8 mm full width at half maximum (FWHM). Experimental runs in which performance in the highest stimulus quality condition dropped below performance in the medium stimulus quality condition, indicating a lack of attention, were excluded from the final analyses. Applying this criterion, for eight participants one run was excluded. For the following analyses different general linear models (GLMs) were constructed that involved parametric regressors of interest, allowing us to disentangle brain regions that tracked the available decision evidence from those that encoded task difficulty due to trial-to-trial effects of noise.

2.4.1. Model 1: stimulus quality

The onsets of piano trials and chair trials were included as separate event regressors, and the standardised level of stimulus quality (i.e., the inverse of the superimposed visual noise for a given run) for piano trials and chair trials were used as additional parametric regressors. Note that the visual noise level was constant for each run, but in the medium noise condition it was adjusted based on participants’ performance accuracy from the previous run. Left and right button presses were modelled as additional regressors-of-no-interest to capture variance related to movement preparation. Head movement parameters were entered as additional co-regressors of no-interest. Group statistical analyses (random effects analyses using the standard summary statistics approach as implemented in SPM8) were performed to test for brain regions in which trial-by-trial activation reflected stimulus quality, applying a threshold of $p < .01$ using family-wise error (FWE) correction for multiple comparisons at voxel level (only clusters > 10 voxels were considered).

2.4.2. Model 2: response times

The onsets of piano trials and chair trials were modelled for each stimulus quality level separately, as well as the standardised response times for piano trials and chair trials as additional regressors, resulting in six boxcar event regressors (onset of the visual stimulation) and six parametric regressors. Button presses and movement parameters were again entered as additional co-regressors-of-no-interest. Group statistical analyses were performed to search for brain regions in which activation reflected response times. Again, a threshold of $p < .01$ (FWE-corrected at voxel level; additional voxel threshold of > 10 voxels) was applied.

2.4.3. fMRI control analyses

In the first control analyses, *performance accuracy* instead of stimulus quality (Model 1) was used as a regressor, to confirm that these models yielded highly similar results, as expected from their strong relationship. In the second control analysis, parametric regressors from both Model 1 (stimulus quality) and Model 2 (response time for constant stimulus quality levels) were entered together in one GLM. This analysis served the purpose of confirming the initial effects. Note that as both main analyses were already conceptually decorrelated as in Model 1, differences in stimulus information were the only driver for neural effects, while in Model 2 such stimulus quality differences were fully eliminated.

2.4.4. Relating fMRI results to DDM parameters

Note that DDM parameters were not directly incorporated into the GLM analysis of the neural data because we could only derive DDM parameters for individuals based on data from the entire experiment, not for single trials. We conducted two sets of analyses in which activation from regions of interest (ROIs) that were found to be modulated by *stimulus quality* or *response time* (with fixed levels of stimulus quality) was correlated with individuals' DDM parameters. Only correlations between neural signals and model parameters, which were not (directly or indirectly) used to define the ROI were considered for these analyses to avoid circularity. Given the relatively low number of participants, which can lead to inflations of p-values, these analyses should be interpreted with caution (Yarkoni, 2009). For regions modulated by *stimulus quality*, we aimed to assess whether additional model-related factors other than stimulus evidence were associated with the neural signals. As the control analysis for the neural signals confirmed that the parametric effects of performance accuracy were nearly identical to those of stimulus quality, and performance accuracy was further highly correlated to drift rates at each level of stimulus quality (see Section 3), this analysis necessarily excluded drift rate (since the available evidence is the main driver for drift rate, and the neural signal of the ROI was chosen to directly reflect this factor, further correlations with drift rate would have been circular). For regions in which the neural signals were modulated by RT independent of stimulus quality, we tested for any residual correlations with model parameters within each stimulus quality level, including drift rates.

For each participant, the model was fit to the choice probabilities and RT distribution data for correct and error responses. Some participants did not produce a sufficient number of errors to estimate the error RT distribution for the easiest discriminability condition—five error RTs are required to estimate five RT quantiles for the errors. For these participants, in this condition only, the overall error rate was used to constrain the parameter estimates alongside the correct RT distribution data. This procedure did not distort the parameter estimates since parameters that were held constant across all discriminability conditions (e.g., boundary separation) impose constraints on parameter estimates for the easiest condition (e.g., drift rate). For each participant, three drift rates ($\boldsymbol{v}$) and three non-decision times ($\boldsymbol{T_{er}}$), one for each difficulty discriminability condition, were estimated. Differences in performance accuracy across discriminability conditions necessitated separate drift rates (which were further required for the correlation analyses). Multiple estimates of non-decision time were required to accommodate a marked slowing of the RTs that occurred in the most difficult discriminability condition, relative to the easier conditions (as well as being required for the correlation analyses). We describe the rationale for using this extended version of the diffusion model in the Section 3. In addition, for each participant, we estimated one boundary separation parameter ($\boldsymbol{a}$), which was held constant across all stimulus conditions, one between-trial drift variability parameter ($\boldsymbol{\eta}$) to account for errors typically being slower than correct responses, as well as one non-decision time variability parameter ($\boldsymbol{s_t}$), and one start-point variability parameter ($\boldsymbol{s_z}$) to account for fast errors (that some, but not all, participants produced). A summary of each participant's total non-decision time ($\boldsymbol{T_{er_total}}$) across stimulus quality conditions was derived by calculating individual regression slopes for the three non-decision times as a function of individuals' performance accuracy for each level. In the same way, we computed summaries of individuals' total drift rates ($\boldsymbol{v_{total}}$) (for details of individual fits to data, see Supplementary material Figs. C.1 and C.2).

3. Results

3.1. Behavioural results

3.1.1. Performance accuracy

A repeated-measures analysis of variance (ANOVA) showed that performance accuracy differed significantly between stimulus quality levels ($F(2,44) = 358.28$; $p < .001$; Fig. 2A). All statistics reported for the following post-hoc tests are Bonferroni-corrected. The difference in performance accuracy between high stimulus quality (M = 87.5% correct, SE = 1.90) and medium stimulus quality (M = 80.0% correct, SE = 1.88) was significant ($t(22) = 9.92$; $p < .001$), and the difference between medium stimulus quality and low stimulus quality (M = 47.4% correct, SE = 0.81) was also significant ($t(22) = 17.76$, $p < .001$). Additional paired-sample *t*-tests showed that there were small but significant differences between object categories, with pianos being correctly identified more often than chairs at high stimulus

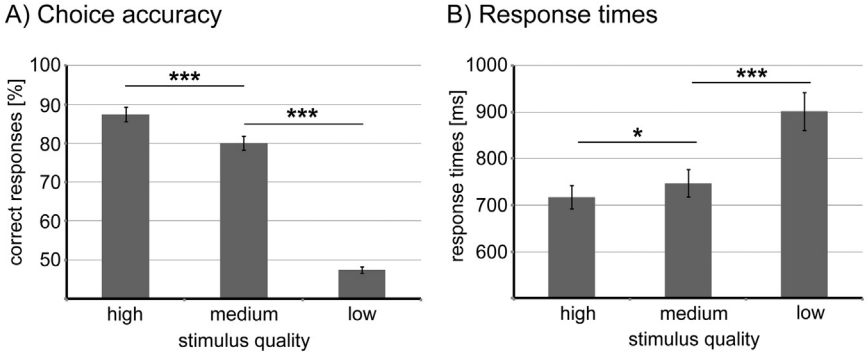

Fig. 2. Behavioural results. A) Average choice accuracies for each stimulus quality condition. Error bars indicate standard errors (SE). Participants performed at ~ 90% accuracy in the high stimulus quality condition, and ~ 50% accuracy in the lowest stimulus quality condition. In the medium stimulus quality condition, performance was close to 80%. Differences between conditions were significant (paired-sample *t*-tests: *** $p < .001$). B) Average response times for each stimulus quality condition. Error bars indicate standard errors (SE). Participants responded fastest in the high stimulus quality condition, followed by the medium stimulus quality condition, and slowest in the low stimulus quality condition. Differences between conditions were significant (paired-sample *t*-tests: * $p < .05$; *** $p < .001$).

quality (chairs: M = 81.8% correct, SE = 2.93; pianos: M = 93.2% correct, SE = 1.31; $t(22) = 4.56$, $p < .001$) and at medium stimulus quality (chairs: M = 71.4% correct, SE = 2.53; pianos: M = 88.7% correct, SE = 1.79; $t(22) = 7.62$, $p < .001$), but not at low stimulus quality (chairs: M = 49.5% correct, SE = 2.66; pianos: M = 45.9% correct, SE = 2.68; $t(22) = 0.7$, $p = .49$). These highly similar choice proportions in the low stimulus quality condition speak against a general choice or preference bias for one or the other category.

3.1.2. Mean response times

A repeated-measures ANOVA on mean RTs replicated the results profile for performance accuracy. Response times differed significantly between stimulus quality levels ($F(2,44) = 17.08$; $p < .001$). All statistics reported for the following post-hoc tests are Bonferroni-corrected. The difference in response times between high stimulus quality (M = 717.4 ms, SE = 23.8) and medium stimulus quality (M = 747.5 ms, SE = 20.6) was significant ($t(22) = 2.48$, $p < .05$), and the difference between medium stimulus quality and low stimulus quality (M = 901.9 ms, SE = 44.4) was also significant ($t(22) = 3.91$, $p < .01$) (Fig. 2B). Additional paired-sample *t*-tests revealed that there were again small but significant differences between object categories, with piano decisions being slightly faster than chair decisions at high stimulus quality (chairs: M = 742.2 ms, SE = 26.7; pianos: M = 692.6 ms, SE = 23.7; $t(22) = 2.92$, $p < .01$) and at medium stimulus quality (chairs: M = 772.6 ms, SE = 22.4; pianos: M = 722.4 ms, SE = 21.7; $t(22) = 3.26$, $p < .01$), but not at low stimulus quality (chairs: M = 910.8 ms, SE = 46.1; pianos: M = 894.2 ms, SE = 44.1; $t(22) = 1.06$, $p = .30$). In sum, piano images were slightly less well masked by our noise mask, but the general experimental manipulation was successful.

3.1.3. DDM fit to behavioural data

We fit the DDM to the choice and RT data from each participant. For each condition, we summarized the information in the correct and error RT distributions using five distribution quantiles: the 0.1, 0.3, 0.5, 0.7, and 0.9 quantiles. Five quantiles suffice to characterize the shape of the distribution while being fairly robust to outliers (Ratcliff and Smith, 2004). The 0.1 quantile characterises the fastest responses in the distribution (the leading edge); the 0.5 quantile characterises its central tendency (the median), and 0.9 quantile characterises the slowest responses (the distribution tail). Parameters were estimated by minimizing the likelihood ratio statistic, G^2,

$$G^2 = 2\sum_{i=1}^{3} n_i \sum_{j=1}^{12} p_{ij} \ln\left(\frac{p_{ij}}{\pi_{ij}}\right),$$

where i indexes the three stimulus quality conditions, j indexes the 12 total response time bins for correct and error responses, p is the predicted proportion of trials, π is the model prediction, and n is the number of trials per condition, which was equal to 144. Because this statistic is computed on the joint distributions of correct responses and errors, it simultaneously fits choice probabilities (response accuracy) and response time distributions.

We fit two versions of the DDM to each participant's data. The first version was a standard implementation of the model, where drift rate was the only parameter that was free to vary across experimental conditions. We found that this version of the model was unable to account for the data from the most difficult discrimination condition, where the fastest RTs were slowed by approximately 75 ms, relative to the other easier conditions. Ratcliff and Smith (2010) reported similar results with simple perceptual stimuli, such as luminance gratings. They found that when stimulus onset was obscured by the presence of dynamic noise, the leading edge of the empirical RT distributions were shifted later in time in a way that could not be accounted for by the standard diffusion model, which only estimates a single T_{er} parameter that applies across all conditions (see also Sewell et al., 2016; Smith et al., 2014, 2016). In our study, the stimuli were more visually complex, comprising degraded images of different piano and chair exemplars. We suggest that when these stimuli are heavily degraded, as was the case in the most difficult condition, it takes longer for people to locate and encode categorically diagnostic feature information from the image, resulting in a delay in the onset of the decision-making process, consistent with previous findings.

To accommodate the shift in the leading edge of the RT data, we considered an extended version of the diffusion model, where we estimated a drift rate and non-decision time for each condition. We compared the fits of the two models using both AIC and BIC, which incorporate different ways of penalizing more complex models. For 22 out of 24 participants, both methods of model selection resulted in the same model being preferred. Under AIC, the extended model was preferred for 20 out of 24 participants (mean difference in AIC = 36.43). Under BIC, the extended model was preferred for 18 out of 24 participants (mean difference in BIC = 28.29). Because the extended model was strongly preferred for the clear majority of participants, we only consider parameter estimates derived from this model in our key analyses. Fit statistics and model predictions for individual participants are provided in the Supplementary material. Table 1 shows the best fitting parameter estimates for the extended model, averaged across individual participants.

The fit of the extended model to the group-averaged data is shown in Fig. 3 in the form of a quantile probability plot. The figure plots RT quantiles for both correct and error responses for each of the three difficulty conditions. For each condition, the correct responses typically appear on the right-hand side of the figure, with a column of plotting symbols above p along the abscissa, where p denotes the proportion of correct responses for that condition. The corresponding error responses from the same condition are plotted above 1-p along the abscissa, so error responses tend to appear on the left-hand side of the figure. The plotting symbols within each column summarize the 0.1, 0.3, 0.5, 0.7, and 0.9 RT quantiles for the relevant distribution (i.e., correct or error responses for a given level of difficulty). The correspondence between the model predictions and the data in Fig. 3 are indicative of the good overall fit when non-decision time is estimated separately for each condition.

3.2. fMRI results

For the following fMRI analyses different general linear models (GLMs) were constructed that involved parametric regressors of interest, allowing us to disentangle brain regions that reflected the available perceptual evidence from those that encoded task difficulty due to trial-to-trial effects of noise in the representation of the stimuli. We first investigated neural effects due to the available stimulus information only. In a separate analysis, we then held stimulus quality constant and investigated neural effects linked to residual variation in response times. In an additional control analysis, we further showed that results from our first analysis were near identical when using

Table 1
Best fitting parameter estimates for the extended diffusion model (Three T_{er}) averaged across participants.

	All	High Stim Qual	Med Stim Qual	Low Stim Qual
v	–	0.334 (0.165)	0.242 (0.137)	− 0.009 (0.016)
a	0.164 (0.030)	–	–	–
T_{er}	–	0.399 (0.064)	0.396 (0.066)	0.476 (0.146)
η	0.215 (0.111)	–	–	–
s_t	0.175 (0.130)	–	–	–
s_z	0.032 (0.068)	–	–	–

Note: Standard deviations are shown in parentheses. v = drift rate; a = boundary separation; T_{er} = non-decision time; η = drift variability; s_t = non-decision time variability; s_z = starting point variability.

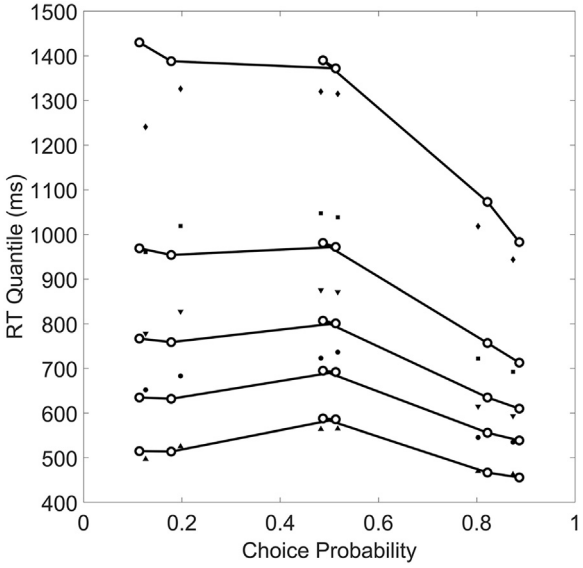

Fig. 3. Fit of the extended diffusion model to the group-averaged data. Model predictions for different quantiles are shown as separate solid lines. The plotting symbols correspond to the different RT quantiles for each of the three difficulty conditions. Note that the model captures the shift in the leading edge of the RT distributions for the most difficult condition (i.e., the middle two columns of plotting symbols). The model handles the shapes of both correct and error responses reasonably well, though the model predicts that the slowest error responses in the easiest condition are slower than are observed empirically (i.e., leftmost column of plotting symbols; prediction line appears above the highest plotting symbol).

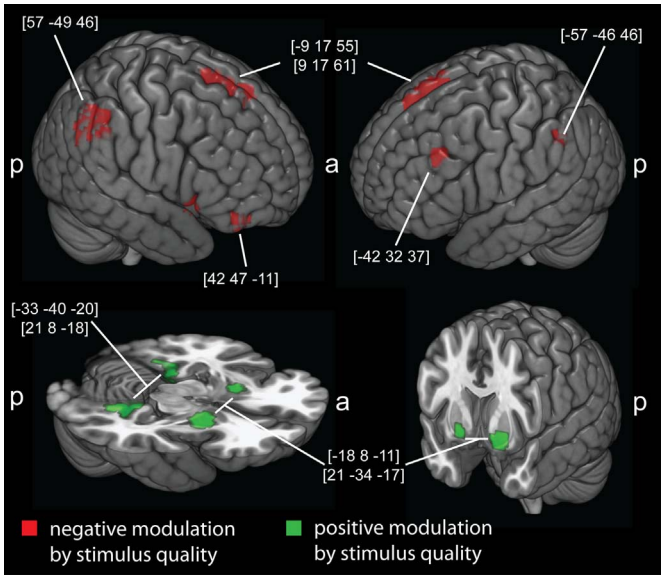

Fig. 4. Results of parametric analyses for stimulus quality. Displayed are regions in which activation significantly reflected stimulus quality on each trial (green: higher stimulus quality levels were associated with stronger activation; red: lower stimulus information levels were associated with stronger activation); $p < .01$, FWE-corrected for all contrasts; a = anterior; p = posterior; see text and tables for statistics. Coordinates are MNI coordinates.

performance accuracy as the parametric regressor instead of stimulus quality, as expected. In the second set of control analyses, we considered both stimulus quality and residual response time variation as independent (and orthogonal) factors in single models.

3.2.1. Parametric modulation by stimulus quality (Model 1)

This analysis showed that the visual stimulation and decision task (onset regressors) generally activated large parts of the brain, with major activation clusters in the visual cortex, the medial temporal lobe, posterior parietal cortex, the basal ganglia, and the left pre-motor and motor cortex (data not shown; the same results were obtained in all other onset analyses).

In the next step, we directly investigated which brain regions reflected *stimulus quality* on each trial. Stronger activation with increasing stimulus quality (i.e., lower levels of visual noise) was found in bilateral ventral temporal cortex, mostly in Brodmann area 37, comprising fusiform gyrus and the parahippocampal gyrus. The other significant clusters were located bilaterally in the putamen/ventral striatum (Table 2, Fig. 4). In a third step, we assessed whether any brain regions showed stronger activation with decreasing stimulus quality (i.e., higher levels of visual noise). This analysis revealed clusters in bilateral supramarginal gyrus, bilateral superior frontal cortex, left middle frontal gyrus and right inferior frontal gyrus (Table 3, Fig. 4). There were no significant general differences in activation between piano and chair stimuli in any brain region, and no differences in the parametric modulation between the two stimulus categories ($p > .01$ uncorrected, for all analyses).

Table 2
Whole brain analysis for positive parametric modulation by *stimulus quality*.

Region	MNI	*t*	*z*	(voxel) *p* <
L vStr	−18 8 −11	6.14	5.75	.0001 FWE
R vStr	21 −34 −17	5.20	4.95	.008 FWE
L ventral temporal cortex	−33 −40 −20	5.32	5.05	.005 FWE
R ventral temporal cortex	21 8 −8	5.24	4.98	.007 FWE

Note: Additional voxel-threshold of 10 voxels applied; R = right; L = left; vStr = ventral striatum; MNI = Montreal Neuroscience Institute coordinates.

Table 3
Whole brain analysis for negative parametric modulation by *stimulus quality*.

Region	MNI	*t*	*z*	(voxel) *p* <
R superior frontal gyrus	9 17 61	7.06	6.49	.0001 FWE
R supramarginal gyrus	57 −49 46	6.39	5.96	.0001 FWE
L supramarginal gyrus	−57 −46 46	5.81	5.48	.0001 FWE
L superior frontal gyrus	−9 17 55	5.80	5.47	.001 FWE
R inferior frontal gyrus	42 47 −11	5.68	5.36	.001 FWE
L middle frontal gyrus	−42 32 37	5.50	5.21	.01 FWE

Note: Additional voxel-threshold of 10 voxels applied; R = right; L = left; MNI = Montreal Neuroscience Institute coordinates.

3.2.2. Control analysis using performance accuracy as regressor

We further confirmed these results by using a complementary model in which instead of stimulus quality, we used the standardised *performance accuracy* (i.e., the percentage of correct responses for this run) for piano and chair trials as parametric regressors. As performance accuracy was expected to be strongly related to stimulus quality (i.e., the higher the stimulus quality, the more accurate the responses should be), these analyses were used to replicate the stimulus quality analyses. As expected, the results closely mirrored results from Model 1 (for details see Supplementary material Tables A.1 and A.2).

3.2.3. Parametric modulation by response time with fixed stimulus quality levels (Model 2)

A positive modulation in all conditions (i.e., stronger activation with faster responses) was found for high stimulus quality in left superior frontal gyrus, bilateral orbitofrontal cortex, extending to the frontal operculum. The last cluster was also found for the low stimulus quality condition (Table 4, Fig. 5). Importantly, the low stimulus quality condition was also the most informative condition, as there were no fluctuations in visual noise across trials, such that fluctuations in RTs cannot be attributed to systematic differences in stimulus information. For the medium stimulus quality level, similar results were

Table 4
Whole brain analysis for positive parametric modulation by *response time*.

Region	MNI	*t*	*z*	(voxel) *p* <
High stimulus quality				
L inferior frontal gyrus	−45 8 31	7.32	6.83	.0001 FWE
R inferior frontal gyrus	42 23 22	5.94	5.66	.0001 FWE
L superior frontal gyrus	−6 23 49	6.86	6.45	.0001 FWE
L insula	−36 26 −2	6.76	6.36	.0001 FWE
R insula	36 26 −2	5.46	5.24	.01 FWE
L inferior parietal lobe	−33 −49 43	5.55	5.32	.001 FWE
Medium stimulus quality				
L inferior frontal gyrus	−45 8 31	7.85	7.26	.0001 FWE
R inferior frontal gyrus	45 26 25	6.47	6.12	.0001 FWE
L superior frontal gyrus	−6 23 46	7.70	7.14	.0001 FWE
L inferior parietal lobe	−36 −49 46	7.48	6.96	.0001 FWE
R inferior parietal lobe	33 −67 40	5.20	5.01	.01 FWE
R insula	36 29 −2	6.53	6.17	.0001 FWE
Low stimulus quality				
L inferior frontal gyrus/insula	−51 14 −2	8.33	7.64	.0001 FWE
R inferior frontal gyrus/insula	51 20 −5	8.20	7.53	.0001 FWE
L inferior parietal lobe	−51 −43 49	7.85	7.26	.0001 FWE
R inferior parietal lobe	51 −46 49	7.33	6.84	.0001 FWE
R superior frontal gyrus	9 14 61	7.51	6.98	.0001 FWE
L middle frontal gyrus	−42 32 37	7.23	6.76	.0001 FWE

Note: Additional voxel-threshold of 10 voxels applied; R = right; L = left; MNI = Montreal Neuroscience Institute coordinates.

obtained that did not reach statistical significance at the strict FWE-corrected threshold. In this condition stimulus quality was adjusted between runs, which might have led to more variability in activation. Significant results for the reverse contrast—stronger activation with slower responses—were found for all three stimulus quality conditions in bilateral inferior frontal gyrus, bilateral superior frontal gyrus, bilateral insula, and left inferior parietal lobe (Table 5 and Fig. 5). There were again no significant differences between object categories in any analysis (all $p > .01$ uncorrected).

3.2.4. Control analyses using both parametric regressors in the same GLM

This control analysis replicated the networks that were positively and negatively modulated by stimulus quality and RT, respectively. This confirmed that the observed effects for RT and stimulus quality were robust (see Supplementary material Table B.1 for details).

3.2.5. Relating fMRI results to DDM parameters

First, BOLD data from all regions of interest (ROIs) that showed significant parametric effects in the above analyses (Figs. 4 and 5) were extracted using the MarsBaR toolbox for SPM (Brett et al., 2002). Individual participants' neural data from the regions showing a modulation by stimulus quality/performance accuracy were then correlated

Table 5
Whole brain analysis for negative parametric modulation by *response time*.

Region	MNI	*t*	*z*	(voxel) *p* <
High stimulus quality				
L superior frontal gyrus	−18 35 58	5.16	4.97	.01 FWE
L/R orbitofrontal cortex	0 29 −5	4.89	4.73	.01 FWE
Medium stimulus quality				
N/A				
Low stimulus quality				
L orbitofrontal cortex	−9 53 −8	5.59	5.35	.001 FWE

Note: Additional voxel-threshold of 10 voxels applied; R = right; L = left; MNI = Montreal Neuroscience Institute coordinates.

with participants' individual model parameters in order to search for additional relations, which were not already captured by the initial parametric BOLD analysis. Note that drift rates at each stimulus quality level were naturally highly correlated with the respective performance accuracy in each stimulus quality condition (high: $r = .68$; $p < .0001$; medium: $r = .50$, $p = .016$; low: $r = .55$, $p = .007$), which was already used to determine the ROIs, and therefore cannot be used for these analyses. It was found that four out of the five regions that were negatively modulated by stimulus quality (red in Fig. 4) showed significant positive correlations with non-decision time variability (s_t), including the right superior frontal gyrus ($r = .70$; $p < .0001$), left superior frontal gyrus ($r = .54$; $p < .008$), right inferior frontal gyrus ($r = .55$; $p = .007$), and right supramarginal gyrus ($r = .44$; $p = .03$). The results for the first three regions also survived Bonferroni-correction (see Supplementary material Fig. C.3 for illustration). The right superior frontal gyrus ($r = .61$; $p = .0019$), the left superior frontal gyrus ($r = .48$; $p < .018$) and right supramarginal gyrus ($r = .42$; $p = .048$) further showed significant correlations with the overall non-decision time (T_{er_total}), but only the results for right superior frontal gyrus survived Bonferroni-correction. In other words, stronger relationships to non-decision time and non-decision time variability were found for regions in which BOLD signals were higher when less perceptual evidence was available. Regions in which activation was positively modulated by stimulus quality (green in Fig. 4) showed no further significant correlations with any model parameters. These findings suggest that activation in regions that were negatively related to available perceptual evidence might have been related to recruiting additional resources for processing difficult stimuli, while regions in which activation was positively related to available evidence did not show such a correlation profile. It should be noted again, however, that due to the low number of participants, which can lead to inflations of p-values in such correlation analyses, these results should nevertheless be interpreted with caution (Yarkoni, 2009).

Finally, we correlated the individual drift rates and non-decision

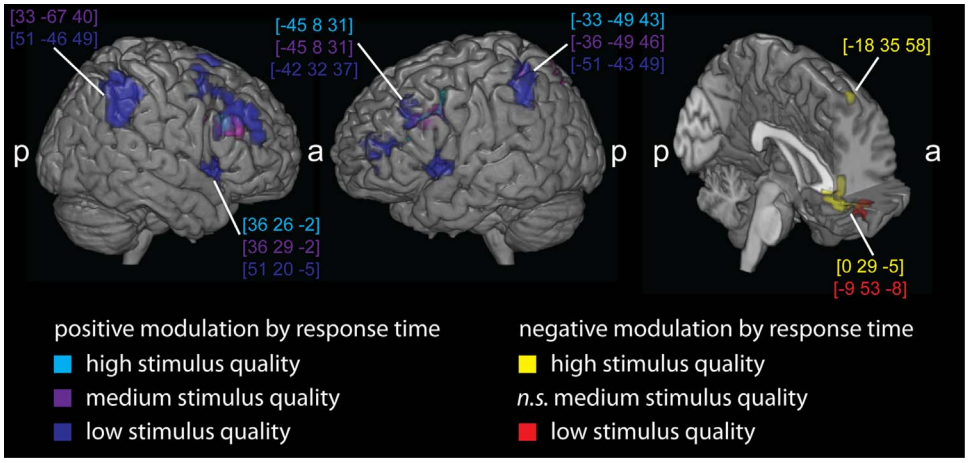

Fig. 5. Results of parametric analyses for response times within stimulus quality level. Displayed are regions in which activation significantly reflected participants' response times (RT), based on separate analyses for each level of stimulus quality. In parietal, lateral prefrontal regions and the insula, activation was significantly associated with slower response times (= positive modulation; blue: low stimulus quality; purple: medium stimulus quality; cyan: high stimulus quality). Regions covering orbitofrontal cortex as well as a cluster in superior frontal gyrus were significantly associated with faster response times (= negative modulation; red: low stimulus quality; medium stimulus quality was not significant; yellow: high stimulus quality); $p < .01$ FWE-corrected for all contrasts; a = anterior; p = posterior; see text and tables for statistics and coordinates for all clusters; coordinates are MNI coordinates.

times for each stimulus quality condition separately with activation from regions for which we found parametric modulation by response time for fixed stimulus quality levels. The orbitofrontal/frontal operculum cluster was the only region in which activation was higher for faster responses (predominately in the high stimulus quality condition) that also showed a significant correlation with drift rate, again exclusively in the high stimulus quality condition ($r = -.48$; $p = .02$). However, this result did not survive Bonferroni-correction. No other significant correlations were found (all $p > .05$), supporting our initial assumption that activity reflecting RT differences in these regions was largely unrelated to differences in available stimulus evidence.

4. Discussion

This study tested whether the effects of stimulus quality and trial-to-trial variability in the encoded representations of stimuli could be dissociated at a neural level using fMRI. For this, we used a task in which participants made perceptual choices between images of pianos and chairs at different discriminability levels. We then used a parametric regression approach and investigated which brain regions were positively or negatively modulated by a) stimulus quality, and b) trial-by-trial response time differences when stimulus quality was held constant. This allowed us to investigate effects of task difficulty due to experimenter-controlled stimulus discriminability, as well as due to the presence of random noise in the representation of stimuli on a given trial. Our analyses for negative associations with stimulus quality and performance accuracy showed a brain network comprising dorsolateral prefrontal cortex (DLPFC), lateral posterior parietal cortex (PPC), medial prefrontal regions (mPFC) including the supplementary motor cortex (SMA) as well as the most anterior part of right inferior frontal gyrus. Highly similar networks were associated with decisions with longer response times when average stimulus quality was fixed: regions comprising DLPFC and lateral PPC were more strongly activated for slower responses, together with clusters in ventrolateral prefrontal cortex (VLPFC) and the insula. When stimulus quality is held constant, slower response times on a given trial are most likely due to the presence of random noise in the representation of choice options, reducing discriminability, and making individual decisions more difficult. This supports the interpretations that these brain networks were recruited when decision difficulty increased, regardless of whether the reason was low stimulus quality or the presence of more random noise. The reverse analyses showed that increasing stimulus quality (across the low, medium and high discriminability conditions) was associated with stronger activation in parts of object-encoding regions in bilateral medial temporal cortex, as well as in the bilateral basal ganglia, mainly the ventral striatum. Finally, across levels of stimulus discriminability, brain regions in orbitofrontal cortex and pre-SMA showed more activation when response times were faster.

4.1. Compensation for different sources of decision difficulty

One of the main findings of our study was that activation in a distinct subset of regions was modulated by decreasing stimulus quality. This network overlapped strongly with regions found by others using similar approaches. For example, Hebart et al. (2012) showed stronger BOLD signals for decreasing motion coherence in their stimuli in several regions, including the anterior cingulate cortex and posterior parietal cortex (see also Kayser et al., 2010a, 2010b). Hebart et al. (2012) also showed that neural signals in parietal cortex allowed for predicting decision outcomes better for less compared to stronger motion coherence, while early visual cortex showed the opposite pattern. It has further been proposed that these regions, particularly PPC and DLPFC, are directly related to perceptual decision-making, potentially in a role such as evidence accumulation and computation of a decision variable (Heekeren et al., 2004, 2006; Ploran et al., 2007, 2011). However, Heekeren et al. (2004) based their argument on the observation that DLPFC was more strongly activated by stronger stimulus evidence, which is the opposite of what we found. Our additional model-based analyses further suggest that activity in this region was related to a longer and more variable non-decision time. One explanation for this might be that on many trials, there was very little (or no) discriminative stimulus information available for decision-making. Consequently, the lack of useful stimulus information may have introduced substantial variation in the efficiency of stimulus encoding (Ratcliff and Smith, 2010). These more difficult decisions may have required recruitment of additional neural resources to support encoding, thereby slowing the onset of the decision process. Instead of being related to the quality of encoded choice options per se, these regions might therefore be more strongly related to *when* the encoded stimulus representations become available to the decision process. Importantly, in our study, most of these regions, in particular PPC, left DLPFC and medial PFC, were also overlapping with those identified in the parametric regression results for slower RTs under constant stimulus quality levels. Because the quality of the evidence was held constant for this analysis, noise fluctuations across trials can account for this finding. This suggests that some trials were more difficult simply because of random variations in the representation of choice options. In support of this interpretation, we did not find any evidence that drift rates (which should be modulated by differences in perceptual evidence) were associated with activation profiles in these areas for fixed stimulus quality levels. Several of these regions have also been found to be modulated by response time variability in an auditory and visual detection task (Walz et al., 2013). This supports the notion that they might reflect, or compensate for, increased difficulty or task demands. This possibility also aligns well with Philiastides and Sajda's (2007) results linking DLPFC to task difficulty, and to attentional effects in PFC and PPC demonstrated by others (Kayser et al., 2010b). This explanation can also be reconciled with the finding that repetitive transcranial magnetic stimulation (rTMS) over DLPFC slowed down response times and increased error rates, suggesting a causal involvement of DLPFC in perceptual decision-making (Philiastides et al., 2011). These rTMS effects on performance do not necessarily require a direct role in evidence accumulation per se, but could alternatively be interpreted as interference with other cognitive functions that ultimately support or influence the decision process. Teichert et al. (2014) recently reported that people sometimes strategically delay the onset of decision-making to improve performance. Whether the same brain regions that are sensitive to RT variability are also implicated in situations involving volitional control of decision onset remains to be tested.

The network described above strikingly resembles the 'multiple demand' (MD) network proposed by Duncan (2010), which also includes PPC, DLPFC, anterior insula, frontal operculum, and pre-SMA, expanding to the ACC (see Fig. 1 in Duncan, 2010). Duncan (2010) points out that this network is consistently found to be activated during a variety of higher cognitive tasks, many of them closely related to decision-making. Duncan (2010) suggests that MD regions are well suited to support sequential, multi-step computations, with a stronger involvement for more demanding tasks. This implies that it is indeed likely that the MD network is part of the decision-making system; but it does not necessarily follow that the MD network should therefore be regarded as the 'seat' of the evidence accumulator. Duncan (2010) noted that these regions are commonly found to be activated together, pointing towards joint task contributions. However, given their individual unique connectivity profiles, it does not seem reasonable to assume that they are functionally identical. Instead, they could be specialised to some degree but in a rather task-general fashion. This is in line with reports that ACC and lateral PFC are involved in conflict detection and cognitive control (Botvinick et al., 2001; Gehring and Knight, 2000), and DLPFC has been implicated in top-down allocation of attention in perceptual choice, even before any information flow from sensory regions to DLPFC takes place (Chand and Dhamala, 2016). The insula may have a role in contributing to the general coupling of

perception to action (Sterzer and Kleinschmidt, 2010). Further, the anterior insula in particular is part of the saliency network, and as such has been found to also activate during very early stages of perceptual decision-making (~ 100 ms post-stimulus), with decision difficulty modulating its causal interactions with other brain regions (Chand and Dhamala, 2016). Lateral PFC and PPC have been shown to represent task rules (Bode and Haynes, 2009; Woolgar et al., 2011), and signals in the posterior parietal cortex have been found to reflect a mixture of choice information, movement preparation and intentional decision plans (e.g., Tosoni et al., 2008). The IFG in particular could subserve internal linguistic processes related to deriving the names of objects (Geva et al., 2011; Morin and Hamper, 2012), or be involved in response inhibition (Keuken et al., 2014). All these functions appear to be components of the decision process that requires sequential accumulation and combination of evidence in a specified task setting; however, the same functions would be required for various other higher cognitive tasks as well.

4.2. Accumulation of stimulus information

Our findings also show that evidence accumulation recruits additional brain regions that showed the opposite activation profiles to those described above, namely, stronger activation with higher stimulus quality. The positive association of stimulus quality (and performance accuracy) with activation in bilateral medial occipito-temporal regions most likely reflects the strength of sensory evidence for the respective objects. Medial ventral temporal cortex could subserve the required comparison of visual input with memory representations of these objects as the same regions have been shown to directly represent object decisions in similar paradigms (Bode et al., 2012a, 2013; see also Philiastides and Sajda, 2007). Interestingly, the second region that showed a highly similar activation profile was mainly located in the ventral striatum. There is increasing evidence of an active role of the basal ganglia in perceptual decision-making (e.g., Bogacz and Gurney, 2007; Forstmann et al., 2010). Some authors have linked ventral striatal regions (together with frontal, parietal and cingulate cortex) to the commitment to a final decision (Costa and Averbeck, 2015). A recent meta-analysis on fMRI studies identified the right putamen as one of the key areas consistently involved in perceptual decision-making (Keuken et al., 2014), but also showed that, as in our study, the putamen was not more strongly activated by more difficult decisions (the reverse contrast was not considered in Keuken et al., 2014). Furthermore, micro-stimulation of caudate neurons in monkeys has been shown to induce choice biases and shifts in RT (Ding and Gold, 2012). These authors noted that the effect of the stimulation “was consistent with an offset in the starting or ending value of an evidence-dependent accumulation process” (Ding and Gold, 2012, p. 869). This suggests a causal role of the basal ganglia, closely linked to the setting of key decision process parameters. In support, the striatum and the strongly interconnected subthalamic nucleus (STN) have been associated with decision threshold settings, which determine the overall cautiousness in responding (e.g., Forstmann et al., 2010; Frank et al., 2015; Herz et al., 2016). We observed a positive modulation of activation in the ventral striatum, which in the context of perceptual decision-making has been implicated in a network involved in action selection, learning and reward prediction (Keuken et al., 2014). Given that higher activation was observed for higher stimulus quality, this might reflect a stronger experience of intrinsic reward on these trials, given that participants could be quite certain about giving a correct response.

Finally, activation in clusters in orbitofrontal cortex and medial prefrontal cortex/pre-SMA was negatively related to RT when stimulus quality was fixed. This means that stronger activation in these regions was observed when decisions were made faster for fixed stimulus quality levels, possibly indicating trials with less random noise in stimulus representations. For the high stimulus quality condition, activation in the orbitofrontal cluster extended posterior, possibly to the frontal operculum, which has been suggested as being related to recognition time (Ploran et al., 2007, 2011). The same authors have also found the pre-SMA to have a highly similar activation profile. We found a correlation between RT-related activation in this region and drift rate in the high stimulus condition (albeit one that did not survive strict Bonferroni-correction), providing some support for the proposed association with recognition time. Orbitofrontal cortex receives inputs from sensory regions, including the visual system, and has been linked to sensory integration, monitoring of performance and outcomes, response inhibition, and decision-making (Elliott et al., 2000; Kringelbach, 2005; Walton et al., 2004), and more recently to representing the hidden states of the task space in order to reach a decision (Schuck et al., 2017). It could therefore play an important role in the commitment to a decision outcome.

4.3. Methodological considerations and limitations

It should be noted that we have assumed that RT variability under constant stimulus quality levels most likely reflects noise in the evidence accumulation process. Evidence accumulation models also allow trial-to-trial variability in decision criteria and variability in the non-decision components of RT. Such variability also has an effect on whether RTs are long or short. When decisions are difficult, accuracy is stressed, and errors are slower than correct responses, the primary determinants of variability in RT are (diffusive) moment-to-moment noise in the accumulation process and across-trial variability in the drift rate (Ratcliff et al., 2016). The effects of variability in starting point are most often seen in tasks in which decisions are easy, speed is stressed, and errors are faster than correct responses (Ratcliff and Smith, 2004). Consistent with this expectation, we did not find any significant correlations of brain activity with variability in starting points. However, activation in some regions seemed to be associated with non-decision time and variability in non-decision time, which points towards variability in the onset of the decision process. Such variability could be related to delays in stimulus encoding due to noise, which would be most pronounced on difficult trials (e.g., Ratcliff and Smith, 2010). Another possible source for RT variation is response conflict, or biases at the level of response selection. Potential biases could originate from conflicts with choices or motor response selection from the previous trials. Our randomised response mappings were designed to eliminate effects of automatic and correlated motor preparation (cf. Bode et al., 2012a; Hebart et al., 2012), but differences in trial-by-trial difficulty (and hence RT when stimulus quality was constant) might, to some extent, also have been driven by random response conflict biases. Thus, while we were unable to provide a strong test for the assumption that RT was mostly affected by sources of noise other than those in the evidence accumulation process, our DDM analyses and the evidence from numerous similar studies suggests that our assumption about the origins of trial-to-trial variability in RT for fixed stimulus quality levels is a reasonable one.

Other computational models for perceptual choice, such as the LBA (Brown and Heathcote, 2008) and the leaky competing accumulator model (Usher and McClelland, 2001) make similar predictions to the DDM, and would need to rely on the same kind of simplifications for a meaningful analysis of the BOLD signal. Given that these models share parameters that perform analogous functions to those in the DDM (e.g., in all three models, choice behaviour is determined by drift rates, decision thresholds, and non-decision time), it is likely that analyses using the LBA or LCA would lead to similar theoretical conclusions (Donkin et al., 2011). We have focussed on the DDM framework here because of its widespread success in accounting for empirical data (Ratcliff et al., 2016), and because it explicitly conceptualises moment-to-moment and trial-to-trial variability in noise, which we could relate to variability in response times. In this study, we have focussed primarily on general aspects of perceptual decisions (stimulus quality and RT variations) that we could directly manipulate or observe (for different approaches see

Tremel and Wheeler, 2015; Frank et al., 2015).

4.4. Dynamics of the decision process

While our results and the results of previous studies (e.g., Philiastides and Sajda, 2006, 2007; Philiastides et al., 2006; Ploran et al., 2007, 2011) clearly point towards specialisation of regions for different aspects of the decision process, it should not be overlooked that the overall picture is that a large network is engaged during the entire decision process. This idea is further supported by electrophysiology studies in monkeys, which have shown that neurons in an extended network of brain regions, spanning from sensory regions, posterior parietal and prefrontal areas to regions related to response preparation, encode decision-relevant information (e.g., Britten et al., 1996; Ding and Gold, 2012, 2013; Gold and Shadlen, 2007; Huk et al., 2017; Kim and Shadlen, 1999; Romo and de Lafuente, 2013; Shadlen and Kiani, 2013; Shadlen and Newsome, 2001). Their relative timing as well as their relative tuning to specific information (e.g., sensory information, decisions, or motor responses) differs; however, most regions have been shown to represent a mixture of this information throughout the entire decision process. This would suggest continuous processing of information that requires the involvement of most of this network at all times, and calls into question whether specific components of the DDM are unambiguously represented in distinct brain regions. Future work would therefore benefit from a stronger focus on investigating how the interplay of different brain regions contributes to evidence accumulation dynamics, which our study did not explicitly address.

4.5. Conclusions

Our study revealed a neural network whose activity is modulated by decision difficulty in two ways. Overlapping parts of this network showed increased activity with a) harder decisions with lower stimulus quality, as well as b) related to trial-by-trial random noise in the representation of choice options for longer response times when stimulus quality was held constant. Our model-based analysis further suggests that the effects found for decreased stimulus information were related to systematic delays in the onset of the decision making process for difficult decisions. Other neural networks were related to the availability of more stimulus evidence and to faster decisions. Our results add to a growing body of evidence suggesting that perceptual decision making shares neural mechanisms with other, similar tasks, and that decision dynamics are better understood as an interaction of network functions (Dmochowski and Norcia, 2015).

Acknowledgements

The authors wish to thank Richard McIntyre, Bowen J. Fung, Christina van Heer, Hayley Warren and Maja Brydevall for help with data acquisition and analysis; and Jutta Stahl and Elaine Corbett for helpful discussions and feedback.

Funding

This work was supported by the University of Melbourne, the Melbourne Neuroscience Institute, the Monash Biomedical Imaging Centre (Monash University), and Australian Research Council Discovery Early Career Researcher Awards to S.B. (DE140100350) and D.K.S. (DE140100772), and an Australian Research Council Discovery Project Grant (DP140102970) to P.L.S. Funding sources had no role in study design, in collection, analysis and interpretation of data, in the writing of the report, and in the decision to submit the article for publication.

Appendix A. Supplementary material

Supplementary data associated with this article can be found in the online version at http://dx.doi.org/10.1016/j.neuropsychologia.2018.01.040.

References

Bennur, S., Gold, J.I., 2011. Distinct representations of a perceptual decision and the associated oculomotor plan in the monkey lateral intraparietal area. J. Neurosci. 31, 913–931.
Binder, J.R., Liebenthal, E., Possing, E.T., Medler, D.A., Ward, B.D., 2004. Neural correlates of sensory and decision processes in auditory object identification. Nat. Neurosci. 7, 295–301.
Bode, S., Bogler, C., Haynes, J.D., 2013. Similar neural mechanisms for guesses and free decisions. Neuroimage 65, 456–465.
Bode, S., Bogler, C., Soon, C.S., Haynes, J.D., 2012a. The neural encoding of guesses in the human brain. Neuroimage 59, 1924–1931.
Bode, S., Haynes, J.D., 2009. Decoding sequential stages of task preparation in the human brain. Neuroimage 45, 606–613.
Bode, S., Sewell, D.K., Lilburn, S., Forte, J., Smith, P.L., Stahl, J., 2012b. Predicting perceptual decision biases from early brain activity. J. Neurosci. 32, 12488–12498.
Bogacz, R., Brown, E., Moehlis, J., Holmes, P., Cohen, J.D., 2006. The physics of optimal decision making: a formal analysis of models of performance in two-alternative forced-choice tasks. Psychol. Rev. 119, 201–215.
Bogacz, R., Gurney, K., 2007. The basal ganglia and cortex implement optimal decision making between alternative actions. Neural Comput. 19, 442–477.
Botvinick, M.M., Braver, T.S., Barch, D.M., Carter, C.S., Cohen, J.D., 2001. Conflict monitoring and cognitive control. Psychol. Rev. 108, 624–652.
Brainard, D.H., 1997. The psychophysics toolbox. Spat. Vis. 10, 433–436.
Brett, M., Anton, J.L., Valabregue, R., Poline, J.B., 2002. Region of interest analysis using an SPM toolbox. In: Proceedings of the 8th International Conference on Functional Mapping of the Human Brain. Neuroimage, 6, 2.
Britten, K.H., Newsome, W.T., Shadlen, M.N., Celebrini, S., Movshon, J.A., 1996. A relationship between behavioral choice and the visual responses of neurons in macaque MT. Vis. Neurosci. 13, 87–100.
Brown, S.D., Heathcote, A., 2008. The simplest complete model of choice response time: linear ballistic accumulation. Cogn. Psychol. 57, 153–178.
Chand, G.B., Dhamala, M., 2016. The salience network dynamics in perceptual decision-making. Neuroimage 134, 85–93.
Costa, V.D., Averbeck, B.B., 2015. Frontal-parietal and limbic-striatal activity underlies information sampling in the best choice problem. Cereb. Cortex 25, 972–982.
Ding, L., Gold, J.I., 2012. Separate, causal roles of the caudate in saccadic choice and execution in a perceptual decision task. Neuron 75, 865–874.
Ding, L., Gold, J.I., 2013. The basal Ganglia's contributions to perceptual decision making. Neuron 79, 640–649.
Ditterich, J., Mazurek, M.E., Shadlen, M.N., 2003. Microstimulation of visual cortex affects the speed of perceptual decisions. Nat. Neurosci. 6, 891–898.
Dmochowski, J.P., Norcia, A.M., 2015. Cortical components of reaction-time during perceptual decisions in humans. PLoS One 10, e0143339.
Donkin, C., Brown, S., Heathcote, A., Wagenmakers, E.J., 2011. Diffusion versus linear ballistic accumulation: different models but the same conclusions about psychological processes? Psychon. Bull. Rev. 18, 61–69.
Duncan, J., 2010. The multiple-demand (MD) system of the primate brain: mental programs for intelligent behaviour. Trends Cogn. Sci. 14, 172–179.
Elliott, R., Dolan, R.J., Frith, C.D., 2000. Dissociable functions in the medial and lateral orbitofrontal cortex: evidence from human neuroimaging studies. Cereb. Cortex 10, 308–317.
Forstmann, B.U., Anwander, A., Schäfer, A., Neumann, J., Brown, S., Wagenmakers, E.J., Bogacz, R., Turner, R., 2010. Cortico-striatal connections predict control over speed and accuracy in perceptual decision making. Proc. Natl. Acad. Sci. USA 107, 15916–15920.
Forstmann, B.U., Dutilh, G., Brown, S., Neumann, J., von Cramon, D.Y., Ridderinkhof, K.R., Wagenmakers, E.J., 2008. Striatum and pre-SMA facilitate decision-making under time pressure. Proc. Natl. Acad. Sci. USA 105, 17538–17542.
Forstmann, B.U., Ratcliff, R., Wagenmakers, E.J., 2016. Sequential sampling models in cognitive neuroscience: advantages, applications, and extensions. Annu. Rev. Psychol. 67, 641–666.
Frank, M.J., Gagne, C., Nyhus, E., Masters, S., Wiecki, T.V., Cavanagh, J.F., Badre, D., 2015. FMRI and EEG predictors of dynamic decision parameters during human reinforcement learning. J. Neurosci. 35, 485–494.
Gehring, W.J., Knight, R.T., 2000. Prefrontal–cingulate interactions in action monitoring. Nat. Neurosci. 3, 516–520.
Geva, S., Jones, P., Crinion, J., Price, C., Baron, J., Warburton, E., 2011. The neural correlates of inner speech defined by voxel-based lesion-symptom mapping. Brain 134, 3071–3082.
Gold, J.I., Shadlen, M.N., 2000. Representation of a perceptual decision in developing oculomotor commands. Nature 404, 390–394.
Gold, J.I., Shadlen, M.N., 2007. The neural basis of decision making. Annu. Rev. Neurosci. 30 (535–374).
Hanks, T.D., Kopec, C.D., Brunton, B.W., Duan, C.A., Erlich, J.C., Brody, C.D., 2015. Distinct relationships of parietal and prefrontal cortices to evidence accumulation. Nature 520, 220–223.

Hebart, M.N., Donner, T., Haynes, J.D., 2012. Human visual and parietal cortex encode visual choices independent of motor plans. Neuroimage 63, 1393–1403.
Hebart, M.N., Schriever, Y., Donner, T.H., Haynes, J.D., 2016. The relationship between perceptual decision variables and confidence in the human brain. Cereb. Cortex 26, 118–130.
Heekeren, H.R., Marrett, S., Bandettini, P.A., Ungerleider, L.G., 2004. A general mechanism for perceptual decision-making in the human brain. Nature 431, 859–862.
Heekeren, H.R., Marrett, S., Ruff, D.A., Bandettini, P.A., Ungerleider, L.G., 2006. Involvement of human left dorsolateral prefrontal cortex in perceptual decision making is independent of response modality. Proc. Natl. Acad. Sci. USA 103, 10023–10028.
Heekeren, H.R., Marrett, S., Ungerleider, L.G., 2008. The neural systems that mediate human perceptual decision making. Nat. Rev. Neurosci. 9, 467–479.
Herz, D.M., Zavala, B.A., Bogacz, R., Brown, P., 2016. Neural correlates of decision thresholds in the human subthalamic nucleus. Curr. Biol. 26, 916–920.
Ho, T.C., Brown, S., Serences, J.T., 2009. Domain general mechanisms of perceptual decision making in human cortex. J. Neurosci. 29, 8675–8687.
Huk, A.C., Katz, L.N., Yates, J.L., 2017. The role of the lateral intraparietal area in (the study of) decision making. Annu. Rev. Neurosci. 40, 349–372.
Kayser, A.S., Buchsbaum, B.R., Erickson, D.T., D'Esposito, M., 2010a. The functional anatomy of a perceptual decision in the human brain. J. Neurophysiol. 103, 1179–1194.
Kayser, A.S., Erickson, D.T., Buchsbaum, B.R., D'Esposito, M., 2010b. Neural representations of relevant and irrelevant features in perceptual decision making. J. Neurosci. 30, 15778–15789.
Keuken, M.C., Müller-Axt, C., Langner, R., Eickhoff, S.B., Forstmann, B.U., Neumann, J., 2014. Brain networks of perceptual decision-making: an fMRI ALE meta-analysis. Front. Hum. Neurosci. 8, 445.
Kim, J.N., Shadlen, M.N., 1999. Neural correlates of a decision in the dorsolateral prefrontal cortex of the macaque. Nat. Neurosci. 2, 176–185.
Kringelbach, M.L., 2005. The human orbitofrontal cortex: linking reward to hedonistic experience. Nat. Rev. Neurosci. 6, 691–702.
Liu, T., Pleskac, T.J., 2011. Neural correlates of evidence accumulation in a perceptual decision task. J. Neurophysiol. 106, 2383–2398.
Luce, R.D., 1986. Response Times. Oxford University Press, New York.
Morin, A., Hamper, B., 2012. Self-reflection and the inner voice: activation of the left inferior frontal gyrus during perceptual and conceptual self-referential thinking. Open Neuroimage J. 6, 78–89.
Philiastides, M.G., Auksztulewicz, R., Heekeren, H.R., Blankenburg, F., 2011. Causal role of dorsolateral prefrontal cortex in human perceptual decision making. Curr. Biol. 21, 980–983.
Philiastides, M.G., Heekeren, H.R., 2009. Spatiotemporal characteristics of perceptual decision making in the human brain. In: Dreher, J.C., Tremblay, L. (Eds.), Handbook of Reward and Decision Making. Academic Press, Burlington, pp. 185–212.
Philiastides, M.G., Ratcliff, R., Sajda, P., 2006. Neural representation of task difficulty and decision making during perceptual categorization: a timing diagram. J. Neurosci. 26, 8965–8975.
Philiastides, M.G., Sajda, P., 2006. Temporal characterization of the neural correlates of perceptual decision making in the human brain. Cereb. Cortex 16, 509–518.
Philiastides, M.G., Sajda, P., 2007. EEG-informed fMRI reveals spatiotemporal characteristics of perceptual decision making. J. Neurosci. 27, 13082–13091.
Pleger, B., Ruff, C.C., Blankenburg, F., Bestmann, S., Wiech, K., Stephan, K.E., Capilla, A., Friston, K.J., Dolan, R.J., 2006. Neural coding of tactile decisions in the human prefrontal cortex. J. Neurosci. 26, 12596–12601.
Ploran, E.J., Nelson, S.M., Velanova, K., Donaldson, D.I., Petersen, S.E., Wheeler, M.E., 2007. Evidence accumulation and the moment of recognition: dissociating perceptual recognition processes using fMRI. J. Neurosci. 27, 11912–11924.
Ploran, E.J., Tremel, J.J., Nelson, S.M., Wheeler, M.E., 2011. High quality but limited quantity perceptual evidence produces neural accumulation in frontal and parietal cortex. Cereb. Cortex 21, 2650–2662.
Purcell, B.A., Heitz, R.P., Cohen, J.Y., Schall, J.D., Logan, G.D., Palmeri, T.J., 2010. Neurally constrained modeling of perceptual decision making. Psychol. Rev. 117, 1113–1143.
Ratcliff, R., 1978. A theory of memory retrieval. Psychol. Rev. 85, 59–108.
Ratcliff, R., McKoon, G., 2008. The diffusion decision model: theory and data for two-choice decision tasks. Neural Comput. 20, 873–922.
Ratcliff, R., Smith, P.L., 2004. A comparison of sequential sampling models for two-choice reaction time. Psychol. Rev. 111, 333–367.
Ratcliff, R., Smith, P.L., 2010. Perceptual discrimination in static and dynamic noise: the temporal relation between perceptual encoding and decision making. J. Exp. Psychol. Gen. 139, 70–94.
Ratcliff, R., Smith, P.L., Brown, S.D., McKoon, G., 2016. Diffusion decision model: current issues and history. Trends Cogn. Sci. 20, 260–281.
Ratcliff, R., Smith, P.L., McKoon, G., 2015. Modeling regularities in response time and accuracy data with the diffusion model. Curr. Dir. Psychol. Sci. 24, 458–470.
Roitman, J.D., Shadlen, M.N., 2002. Response of neurons in the lateral intraparietal area during a combined visual discrimination reaction time task. J. Neurosci. 22, 9475–9489.
Romo, R., de Lafuente, V., 2013. Conversion of sensory signals into perceptual decisions. Prog. Brain Res. 103, 41–75.
Romo, R., Salinas, E., 2003. Flutter discrimination: neural codes, perception, memory and decision making. Nat. Rev. Neurosci. 4, 203–218.
Selen, L.P., Shadlen, M.N., Wolpert, D.M., 2012. Deliberation in the motor system: reflex gains track evolving evidence leading to a decision. J. Neurosci. 32, 2276–2286.
Serences, J.T., Boynton, G.M., 2007. The representation of behavioural choice for motion in human visual cortex. J. Neurosci. 27, 12893–12899.
Sewell, D.K., Lilburn, S.D., Smith, P.L., 2016. Object selection costs in visual working memory: a diffusion model analysis of the focus of attention. J. Exp. Psychol. Learn. Mem. Cogn. 42, 1673–1693.
Sewell, D.K., Smith, P.L., 2016. The psychology and psychobiology of simple decisions: speeded choice and its neural correlates. In: Montag, C., Reuter, M. (Eds.), Neuroeconomics. Springer, Berlin, pp. 253–292.
Shadlen, M.N., Kiani, R., 2013. Decision making as a window on cognition. Neuron 80, 791–806.
Shadlen, M.N., Newsome, W.T., 2001. Neural basis of a perceptual decision in the parietal cortex (area LIP) of the rhesus monkey. J. Neurophysiol. 86, 1916–1936.
Smith, P.L., Lilburn, S.D., Corbett, E.A., Sewell, D.K., Kyllingsbæk, S., 2016. The attention-weighted sample-size model of visual short-term memory: attention capture predicts resource allocation and memory load. Cogn. Psychol. 89, 71–105.
Smith, P.L., Ratcliff, R., 2004. Psychology and neurobiology of simple decisions. Trends Neurosci. 27, 161–168.
Smith, P.L., Ratcliff, R., 2015. Diffusion and random walk processes. In: Wright, J.D. (Ed.), International Encyclopedia of the Social & Behavioral Sciences. Elsevier, Oxford, pp. 395–401.
Smith, P.L., Ratcliff, R., Sewell, D.K., 2014. Modeling perceptual discrimination in dynamic noise: time-changed diffusion and release from inhibition. J. Math. Psychol. 59, 95–113.
Sterzer, P., Kleinschmidt, A., 2010. Anterior insula activations in perceptual paradigms: often observed but barely understood. Brain Struct. Funct. 214, 611–622.
Teichert, T., Ferrera, V.P., Grinband, J., 2014. Humans optimize decision-making by delaying decision onset. PLoS ONE 9 (3), e89638.
Tosoni, A., Galati, G., Romani, G.L., Corbetta, M., 2008. Sensory-motor mechanisms in human parietal cortex underlie arbitrary visual decisions. Nat. Neurosci. 11, 1446–1453.
Townsend, J.T., Ashby, F.G., 1983. Stochastic Modeling of Elementary Psychological Processes. Cambridge University Press, Cambridge.
Tremel, J.J., Wheeler, M.E., 2015. Content-specific evidence accumulation in inferior temporal cortex during perceptual decision-making. Neuroimage 109, 35–49.
Tsunada, J., Liu, A.S.K., Gold, J.I., Cohen, Y.E., 2016. Causal contribution of primate auditory cortex to auditory perceptual decision-making. Nat. Neurosci. 19, 135–142.
Schuck, N.W., Cai, M.B., Wilson, R.C., Niv, Y., 2017. Human orbitofrontal cortex represents a cognitive map of state space. Neuron 91, 1402–1412.
Usher, M., McClelland, J.L., 2001. The time course of perceptual choice: the leaky, competing accumulator model. Psychol. Rev. 108, 550–592.
Vickers, D., 1979. Decision Processes in Visual Perception. Academic Press, New York.
Walton, M.E., Devlin, J.T., Rushworth, M.F., 2004. Interactions between decision making and performance monitoring within prefrontal cortex. Nat. Neurosci. 7, 1259–1265.
Walz, J.M., Goldman, R.I., Carapezza, M., Muraskin, J., Brown, T.R., Sajda, P., 2013. Simultaneous EEG-fMRI reveals temporal evolution of coupling between supramodal cortical attention networks and the brain stem. J. Neurosci. 33, 19212–19222.
Watson, A.B., Pelli, D.G., 1983. QUEST: a Bayesian adaptive psychometric method. Percept. Psychophys. 33, 113–120.
Williams, M.A., Dang, S., Kanwisher, N.G., 2007. Only some spatial patterns of fMRI response are read out in task performance. Nat. Neurosci. 10, 685–686.
Woolgar, A., Thompson, R., Bor, D., Duncan, J., 2011. Multi-voxel coding of stimuli, rules, and responses in human frontoparietal cortex. Neuroimage 56, 744–752.
Yarkoni, T., 2009. Big correlations in little studies: inflated fMRI correlations reflect low statistical power – commentary on Vul et al. (2009). Perspect. Psychol. Sci. 4, 294–298.

Supplementary Material:

Dissociating neural variability related to stimulus quality and response times in perceptual decision-making

Stefan Bode[a,b]*, Daniel Bennett[a,c,d], David K. Sewell[a,e], Bryan Paton[f,g,h,i], Gary F. Egan[f,g,h], Philip L. Smith[a], and Carsten Murawski[c]

[a] Melbourne School of Psychological Sciences, The University of Melbourne, Australia
[b] Department of Psychology, University of Cologne, Germany
[c] Department of Finance, The University of Melbourne, Australia
[d] Princeton Neuroscience Institute, Princeton University, New Jersey, USA
[e] School of Psychology, The University of Queensland, Australia
[f] Monash Biomedical Imaging, Monash University, Australia
[g] School of Psychological Sciences, Monash University, Australia
[h] ARC Centre of Excellence for Integrative Brain Function, Monash University, Australia
[i] School of Psychology, The University of Newcastle, Australia

*** Corresponding Author:**
Stefan Bode, PhD
Decision Neuroscience Laboratory
Melbourne School of Psychological Sciences
The University of Melbourne, Parkville, VIC, 3010, Australia
Email: sbode@unimelb.edu.au
Phone: +61 (0)3 9035 3849

A. Control fMRI analyses: Parametric modulation by performance accuracy

Methods

Performance accuracy: The model for performance accuracy was complementary to Model 1 *(stimulus quality model)*, and served as a confirmation of the results from that model. The onsets of piano trials and chair trials were included as regressors, and the standardised performance accuracy (i.e., the percentage of correct responses for a run) for piano and chair trials was used as an additional parametric regressor. For each run, performance accuracy was calculated for all stimulus quality levels separately, meaning that it varied between runs within each stimulus quality level. Left and right button presses were modelled as additional regressors-of-no-interest, and movement parameters were also entered as additional co-regressors-of-no-interest. The same group statistical analyses were performed as for Model 1 to search for brain regions in which trial-by-trial activation reflected performance accuracy.

Results

Significant positive parametric modulation of brain activation *with performance accuracy* closely mirrored the parametric *stimulus quality* analysis. Activation was again found to be increased with increased performance accuracy in the same cluster in the bilateral ventral temporal cortex, mostly Brodmann area 37, comprising fusiform gyrus and the parahippocampal gyrus. The other significant clusters were again located bilaterally in the ventral striatum (for details see Table A.1). Stronger activation with decreasing performance accuracy was found in the same clusters in bilateral supramarginal gyrus, bilateral superior frontal cortex, left middle frontal gyrus and right inferior frontal gyrus (all $p < .01$, FWE-corrected at voxel level; see Table A.2). There were no significant differences between object categories in any of these analyses (all $p > .01$ uncorrected).

Table A.1: Whole brain analysis for positive parametric modulation by *performance accuracy*

Region	**MNI**	***t***	***z***	**(voxel) *p* <**
L vStr	-18 8 -11	5.50	5.21	.002 FWE
R vStr	18 11 -8	4.33	4.18	.17 FWE (.0001 uncorr)
L ventral temporal cortex	-21 -37 -17	4.87	4.66	.03 FWE
R ventral temporal cortex	27 -40 -17	4.62	4.44	.07 FWE (.00001 uncorr)

Note: Additional voxel-threshold of 10 voxels applied; R = right; L = left; MNI = Montreal Neuroscience Institute coordinates; vStr = ventral striatum.

Table A.2: Whole brain analysis for negative parametric modulation by *performance accuracy*

Region	**MNI**	***t***	***z***	**(voxel) *p* <**
R superior frontal gyrus	9 17 61	6.26	5.84	.0001 FWE
R supramarginal gyrus	60 -40 46	5.79	5.46	.001 FWE
L supramarginal gyrus	-54 -46 46	5.58	5.28	.01 FWE
L/R superior frontal gyrus	3 35 55	5.37	5.10	.01 FWE
R inferior frontal gyrus	39 47 -11	5.33	5.06	.01 FWE
L middle frontal gyrus	-42 32 37	5.10	4.87	.01 FWE

Note: Additional voxel-threshold of 10 voxels applied; R = right; L = left; MNI = Montreal Neuroscience Institute coordinates.

B. Control fMRI analyses: Parametric modulation by stimulus quality and response times in a single model

Methods

In order to confirm that our results from Model 1 (*stimulus quality*) and Model 2 (r*esponse time*) reflected robust effects of both parametric regressors, we conducted additional analyses in which both parametric regressors were entered together (each orthogonalised to the other in two independent analyses). All other aspects of the model were identical to the main models, and left and right button presses were again modelled separately as additional regressors-of-no-interest, and head movement parameters were entered as additional co-regressors-of-no-interest. The same statistical threshold of $p < .01$ (FWE-corrected at voxel level; additional voxel threshold of >10 voxels) was applied for group-level analyses.

Results

The regions revealed in this analysis were largely identical to both separate analyses (see main text). Table B.1 reports the results for both analyses, first when *Stimulus Quality* was the interpretable regressor (top), and below when *Response Time* was the interpretable regressor (bottom). When response time was entered as the first parametric regressor, the positive modulation by response time (RT) (stronger activation for slower responses) explained most of the variance in the prefrontal-parietal network. When stimulus quality was entered as the first parametric regressor, the effects for the positive modulation by stimulus quality remained significant ($p < .01$, FWE-corrected at voxel-level). Taken together, this analysis confirmed that the observed parametric effects for RT and stimulus quality were robust.

Table B.1: Whole brain analysis for positive and negative parametric modulation by *stimulus quality* and *response time* as orthogonal regressors

Stimulus quality – positive modulation				
Region	**MNI**	***t***	***z***	**(voxel) *p* <**
L vStr	-18 8 -11	5.66	5.29	.001 FWE
R vStr	21 14 -2	5.11	4.83	.001 FWE
L ventral temporal cortex	-33 -40 -20	5.38	5.06	.01 FWE
R ventral temporal cortex	30 -40 -17	5.24	4.94	.001 FWE
Stimulus quality – negative modulation				
Region	**MNI**	***t***	***z***	**(voxel) *p* <**
R superior frontal gyrus/middle front. gyrus	6 20 64	7.13	6.45	.0001 FWE
R supramarginal gyrus	63 -37 43	6.02	5.58	.0001 FWE
L supramarginal gyrus	-54 -43 43	5.42	5.09	.01 FWE
L superior frontal gyrus/middle front. gyrus	-9 17 55	5.88	5.47	.001 FWE
R inferior frontal gyrus / insula	54 20 -5	5.75	5.37	.001 FWE
Response time – positive modulation				
Region	**MNI**	***t***	***z***	**(voxel) *p* <**
L inferior frontal gyrus / insula	-51 14 -2	9.25	7.57	.0001 FWE
R inferior frontal gyrus / insula	51 20 -2	7.90	7.01	.0001 FWE
L inferior parietal lobe	-36 -49 43	8.61	7.51	.0001 FWE
R inferior parietal lobe	45 -43 52	6.74	6.15	.0001 FWE
L middle frontal gyrus	-39 26 28	7.95	7.05	.0001 FWE
R middle frontal gyrus	48 26 25	8.74	7.60	.0001 FWE
L/R medial frontal gyrus / ACC	-6 23 46	9.67	7.58	.0001 FWE
Response time – negative modulation				
Region	**MNI**	***t***	***z***	**(voxel) *p* <**
L orbitofrontal cortex	-12 47 -8	5.37	5.05	.01 FWE

Note: Additional voxel-threshold of 10 voxels applied; R = right; L = left; MNI = Montreal Neuroscience Institute coordinates; vStr = ventral striatum.

C. Individual modelling of behavioural data

We contrasted the fits of two versions of the diffusion decision model (DDM) to the individual participant data (see main text for details about the models and fitting procedure). Briefly, the two versions we considered were a standard implementation of the model, where only drift rate varied across conditions, and an extended version of the model where drift rate and non-decision time were both allowed to vary across conditions. The latter model was considered because of the presence of a marked slowing in the leading edge of the RT distribution data for the most difficult condition. Ratcliff and Smith (2010) reported a similar finding, and showed that the standard version of the model failed to accommodate the shift in the leading edge. We used AIC and BIC to contrast the fits of the two versions of the DDM, and found that the extended model provided a superior fit for the vast majority of participants (i.e., 18 out of 24 under BIC and 20 out of 24 under AIC). Individual fit results are reported in Table C.1.

Table C.1. Model fits (G^2) and AIC and BIC for the two versions of the diffusion model tested.

	Extended Model (Three T_{er})			Standard Model		
Participant	G^2	AIC	BIC	G^2	AIC	BIC
1	34.38	54.38	***95.06***	85.88	101.88	134.42
2	54.03	74.03	114.72	54.88	70.88	***103.42***
3	32.84	52.84	93.52	33.92	49.92	***82.47***
4	107.59	127.59	**168.27**	181.76	197.76	230.31
5	61.10	81.10	***121.78***	74.75	90.75	123.30
6	99.15	119.14	**159.83**	169.06	185.06	217.61
7	17.75	37.75	78.43	21.09	37.09	***69.63***
8	48.13	68.13	**108.82**	75.98	91.98	124.53
9	18.24	38.24	***78.92***	71.33	87.33	119.88
10	67.12	87.12	127.80	73.01	89.01	**121.56**
11	66.81	86.81	**127.50**	82.18	98.18	130.73
12	104.38	124.38	***165.06***	206.72	222.72	255.27
13	29.75	49.75	***90.43***	80.41	96.41	128.95
14	55.21	75.21	***115.90***	121.21	137.21	169.75
15	47.03	67.03	***107.71***	90.85	106.85	139.40
16	50.01	70.01	***110.70***	130.21	146.21	178.75
17	19.44	39.44	80.13	19.59	35.59	***68.13***
18	55.13	75.13	***115.81***	112.25	128.25	160.80
19	45.83	65.83	**106.52**	60.40	76.40	108.95
20	33.68	53.68	***94.37***	101.04	117.04	149.59
21	57.91	77.91	***118.60***	125.70	141.71	174.25
22	42.51	62.51	***103.20***	119.61	135.61	168.16
23	76.70	96.70	***137.38***	96.33	112.33	144.88
24	34.17	54.17	94.85	41.04	57.04	***89.59***

Note: The preferred model under BIC is shown in bold and italicized. The preferred model under AIC is underlined. Both methods of model selection agree for 22 out of 24 participants.

The results of the model comparison showed that the extended version of the DDM was preferred for most participants. The fit of the model to the group-averaged data is described in the main text. Overall, the DDM successfully accounted for the differences in the shapes of RT distributions for correct responses and errors as a function of stimulus quality level as well as the differences in choice probability with three drift rates and three non-decision times for all participants. Figure C.1 displays the individual fits for the RT quantile predictions, and Figure C.2 displays the individual fits for the accuracy predictions. These figures plot predicted against observed data, and so the diagonal line in each panel shows when model predictions exactly match the data. The tight clustering of the data around the diagonal shows that, for both RTs and choice probabilities, the model does an excellent job capturing the patterns of data at the

individual level. The model parameters were therefore used in correlation analyses with BOLD data. The methods and results of these analyses are reported in the main manuscript, and the significant correlations are illustrated in Figure C.3.

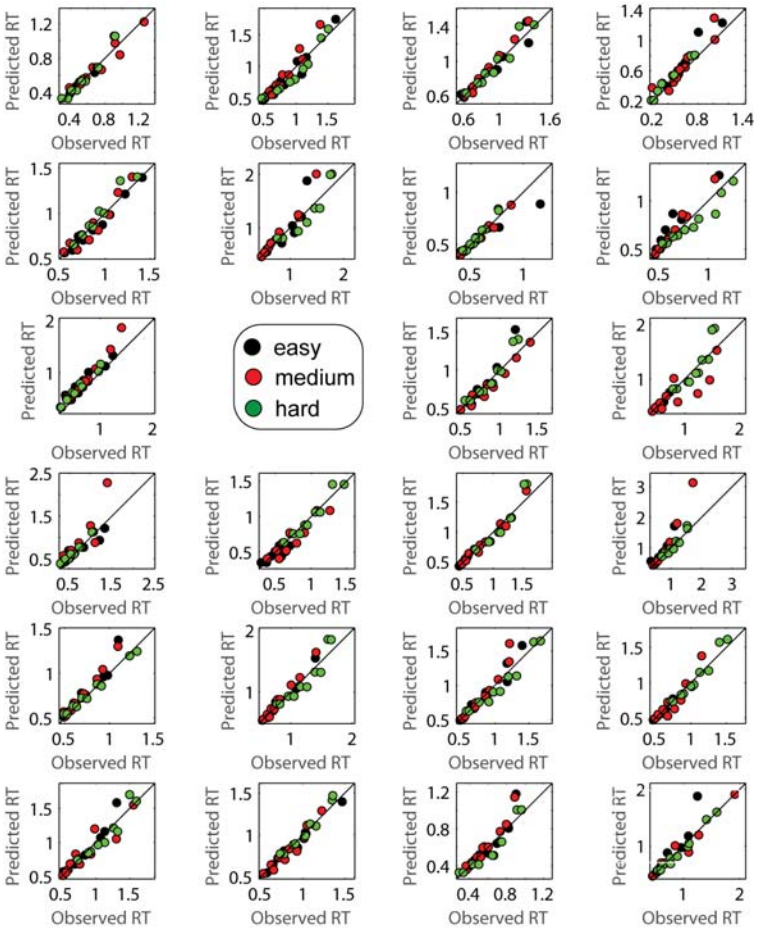

Figure C.1: The figure shows the observed response times (RT; x-axis) and the predicted RT (y-axis) of the extended diffusion model for each participant. Data from easy trials (high stimulus quality) are shown in black, from medium trials (medium stimulus quality) in red, and from hard trials (low stimulus quality) in green.

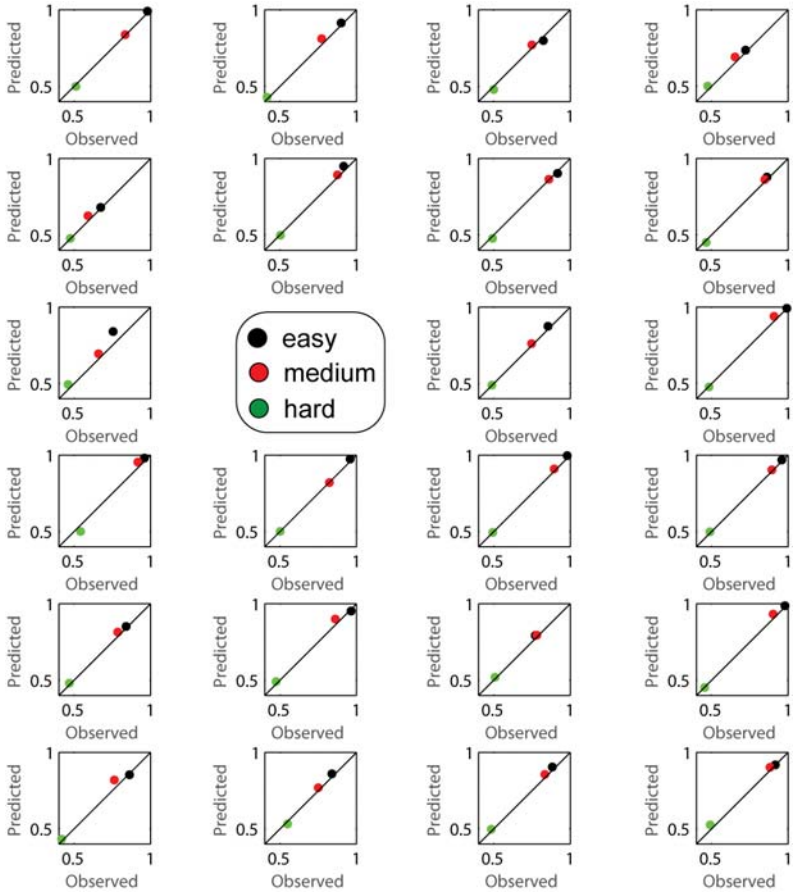

Figure C.2: The figure shows the observed accuracies (x-axis) and the predicted accuracies (y-axis) of the extended diffusion model for each participant. Data from easy trials (high stimulus quality) are shown in black, from medium trials (medium stimulus quality) in red, and from hard trials (low stimulus quality) in green.

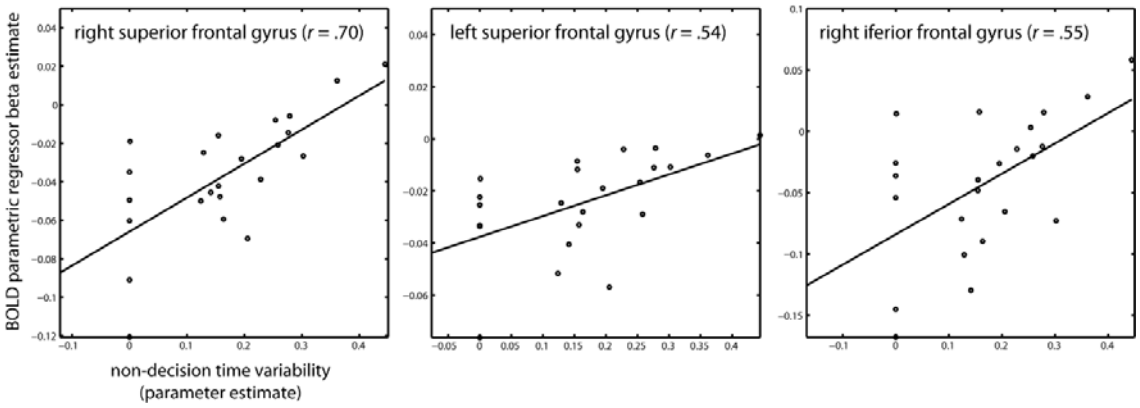

Figure C.3: Illustration of correlations between individual BOLD parametric regression coefficients and non-decision time variability coefficients (only correlations that survived Bonferroni-corrections are shown). See main text for details.

References for Supplementary Material

Ratcliff, R., Smith, P.L., 2010. Perceptual discrimination in static and dynamic noise: the temporal relation between perceptual encoding and decision making. J. Exp. Psychol. Gen. 139, 70–94.